



**REAL-TIME MODULATED NANOPARTICLE SEPARATION
WITH AN ULTRA-LARGE DYNAMIC RANGE**

Journal:	<i>Lab on a Chip</i>
Manuscript ID	LC-ART-09-2015-001051.R1
Article Type:	Paper
Date Submitted by the Author:	26-Oct-2015
Complete List of Authors:	Kwek, Kerwin Zeming; National University of Singapore, Singapore Institute of Neurotechnology Thakor, Nitish; National University of Singapore, Singapore Institute of Neurotechnology; Johns Hopkins University School of Medicine, Department of Biomedical Engineering Zhang, Yong; National University of Singapore, Department of Biomedical Engineering; National University of Singapore, Cellular and Molecular Bioengineering lab Chen, Chia-Hung; National University of Singapore, Department of Biomedical Engineering; National University of Singapore, Singapore Institute of Neurotechnology

REAL-TIME MODULATED NANOPARTICLE SEPARATION WITH AN ULTRA-LARGE DYNAMIC RANGE

Kerwin Kwek Zeming^a, Nitish V. Thakor^{a,b}, Yong Zhang^{c,d}, Chia-Hung Chen^{a,c*}*

Author affiliation:

a: Singapore Institute for Neurotechnology (SINAPSE), 28 Medical Dr. #05-COR, Singapore 117456

b: Department of Biomedical Engineering, Johns Hopkins University School of Medicine, Traylor 701 / 720 Rutland Ave, Baltimore, MD 21205

c: Department of Biomedical Engineering, National University of Singapore, 9 Engineering Drive 1, Block EA #03-12, Singapore 117576,

d: Cellular and Molecular Bioengineering Lab, National University of Singapore, Block E3A, #07-06, 7 Engineering Drive 1, Singapore 117574

*Corresponding Authors:

Yong Zhang

Department of Biomedical Engineering,
National University of Singapore,
9 Engineering Drive 1, Block EA #03-12, Singapore 117576
+65 6516 4871
biezy@nus.edu.sg

Chia-Hung Chen

Department of Biomedical Engineering,
National University of Singapore,
9 Engineering Drive 1, Block EA #03-12, Singapore 117576
+65 98514596
biecch@nus.edu.sg

Keywords

Deterministic lateral displacement, nanoparticle separation, Debye length, electrostatic charge, electric double layer, apparent particle size

Abstract

Nanoparticles exhibit size-dependent properties which makes size-selective purification of proteins, DNA or synthetic nanoparticles essential for bio-analytics, clinical medicine, nanoplasmonics and nano-material sciences. Current purification methods of centrifugation, column chromatography and continuous-flow techniques suffer from particle aggregation, multi-stage process, complex setups and necessary nanofabrication. These increase process costs, time, reduce efficiency and limit dynamic range. Here, we achieve unprecedented real-time nanoparticle separation (51nm – 1500nm) using large-pore (2 μm) deterministic lateral displacement device (DLD). No external force-fields or nanofabrication are required. Instead, we investigated innate long-ranged electrostatic influences on nanoparticles within a fluid medium at different NaCl ionic concentrations. In this study we account for the electrostatic forces beyond Debye length and showed that it cannot be assumed as negligible especially for precise nanoparticle separation methods such as DLD. Our findings have enabled us to develop a model to simultaneously quantify and modulate the electrostatic force interactions between nanoparticle and micropore. By simply controlling buffer solutions, we achieve dynamic nanoparticle size separation on a single device with a rapid response time (< 20 s) and an enlarged dynamic range (> 1200%), outperforming standard benchtop centrifuge system. This novel method and model combines device simplicity, isolation precision and dynamic flexibility, opening opportunities for high-throughput applications in nano-separation for industrial and biological applications.

Introduction

Nanoparticles exhibit size-dependent properties based on their morphology, structure, chemical composition and synthesis process¹⁻³. The size-selective purification of nanoscopic objects is essential for a broad spectrum of applications in bio-analytics, clinical medicine, bead-based assays, high-resolution optical imaging, nanoparticle catalytic activity and nanocomposite materials in which the nanoparticle size determine the overall properties such as antibacterial functions⁴⁻⁸. Conventional methods for nanoparticle separation and purification, such as gel electrophoresis, column chromatography and centrifugation, have high separation resolutions and well-established protocols⁹; however, they require multistage extraction processes without real-time control over particle separation, which inevitably limits the dynamic range of nanoparticle separation that can be achieved. For instance, the affinity binding chromatography method of purifying proteins or drugs requires multiple processing steps for column preparation, sample binding, washing, eluting and purification for a period of 12 to 48 hours. Centrifugal systems are the most common method of purifying nanoparticles because they offer highly reproducible separation based on particle size and density^{10,11}. However, without continuous flow separation, sample loss occurs due to nanoparticle aggregation and the difficulty of re-suspending a centrifuged sample¹².

Continuous flow separation is a new class of separation that can be achieved using microfluidic devices. It is low in cost and offers reduced sample/reagent requirements, scalable throughput, device automation and real-time control of the separation ranges^{13,14}. A wide spectrum of methods ranging from active acoustic^{15,16}, electrophoretic¹⁷, and centrifugal¹⁸ force fields to passive pore-based filtration¹⁹ and nano-structured traps²⁰ have been developed for

nanoparticle separation in fluidic devices. Among these methods, pore-based deterministic lateral displacement (DLD) method is highly promising due to its versatility for passive or integrated active sorting modes, scalability and potential nanometer-resolution separation^{16,21-23}. Attempts have been made to use DLD for nano-separation, but the results showed poor separation of 190 nm particle separations²⁴. To date, Huang et al. have succeeded in electrokinetically separating large bacterial DNA using DLD devices characterized by nanometer-scale polystyrene particles ranging from 1000 nm to 600 nm²¹; Chen et al. separated a 1000 nm blob of genomic DNA using a 1.7 μm DLD pore in a high concentration of polyethylene-glycol (10% w/v)²⁵. Despite these advances, effective continuous flow nano-separation is highly dependent on active force fields or nano-fabricated constructs, resulting in a trade-off between dynamic range and separation resolution. Active force fields allow for real-time particle separation manipulation, although achieving high-resolution separation remains challenging and additional equipment is required. By contrast, nano-fabricated constructs enable remarkable control over separation resolution, albeit with limited dynamic range control, complex nano-lithography requirements and low throughput.

In this study, we explore a novel nano-separation method based on real-time nano-particle size modulation in micro-fabricated DLD devices without applying any external force field. We managed to separate a large range of particle sizes from 51 nm to 1500 nm in a single DLD device. We modulate the nanoparticle size by simply changing buffer reservoir solution with different ionic concentrations. Differing salt ionic concentration creates different thickness of electric double layer (EDL) which modulates the electrostatic force interactions between the nanoparticle and walls of the DLD device (Fig 1.)²⁶. The nanoparticle displacement induced by

the electrostatic and hydrodynamic forces alters the apparent size of the particle for nano-separation in DLD devices. Accordingly, the sizes of the separated nanoparticles can therefore be regulated by adjusting the ionic concentration of the buffer.

Notably, modifying the buffer's ionic concentration can actively modulate nanostructure and nanoparticle interactions²⁷⁻³¹. Fu et al.³⁰ and Regtmeier et al.³¹ have explored similar ionic methods of modulating overlapping Debye layers to control nanofluidic pore sizes for selective particle separation. The Debye length is the characteristic parameter that is used to approximate the EDL thickness within these pores and nanostructures. Fu et al. successfully separated DNA and proteins using a pore size of 300 nm, whereas Regtmeier et al. separated 15 nm particles using a 515 nm gap. However, in both works, an external electric field source was necessary to electrokinetically drive the separation of the particles. These systems do not permit the adjustment of the buffer's ionic concentration in real time and require the fabrication of nanoscale gaps, thereby restricting device throughput and dynamic range. Moreover, Debye length approximations of particle and pore interactions understate the true EDL effects. Thus, a novel model to account for the long range electrostatic effects is explored here in addition to the real-time nanoparticle size modulation for precision separation control.

By developing the model, the novelty of this communications is two-fold, 1) we precisely predict and control the long-range EDL electrostatic effects on particle in fluid medium to control the particle apparent size. 2) This enable us to develop a method for continuous flow real-time nano-separation modulation without the use of external force fields in micro-fabricated DLD systems. By changing the apparent particle size through the injection of ionic buffer solutions, the dynamic range was significantly amplified (> 1200%), increasing the pore-

to-particle size ratio (~40 times). Dynamic nano-separation was demonstrated to discriminate a spectrum of particles with varied diameters (51 nm to 1,500 nm) within a rapid response time of less than 20 seconds. To our knowledge, there are no other methods that offer sufficiently precise separation and dynamic flexibility to separate particles with sizes ranging from 51 nm to the micron scale under continuous flow conditions²⁴. The modulated separation of 51 nm polystyrene particles outperformed a conventional bench-top centrifugal system. The size modulation of the nanoparticles was achieved by simply changing the ionic concentration of the buffer reservoir solution. With future refinements and scaling up of the device, high-throughput nano-separation for industrial applications can be approached, and precise diagnoses can be achieved based on the isolation of circulating biomarkers such as viruses, exosomes, proteins and DNA.

Materials and methods

The DLD device

The DLD method for particle separation in microfluidic devices has been extensively studied for the past decade, since it was first reported by Huang et al.²¹. DLD is a continuous flow separation technique based on a pillar array gradient that determines the displacement of a particle in the lateral direction. The critical cut-off size for the particles is determined by the gradient and the gap between adjacent pillars in the array. Particles larger than the critical cut-off diameter (D_c) will be displaced from the sample streamline, whereas smaller particles will seemingly flow unhindered through the pillar array by traveling within the fluid streamlines. The empirical formula derived by Davis et al.³² is found in Eq. 1.

In this paper, all DLD devices discussed are multi-segmented devices with 14 critical diameter segments, as shown in Fig. 2(d), with each segment in a continuous sequence. Each DLD segment is responsible for the lateral displacement of particles of a specific size, and these particles will exit at their respective outputs (Fig. 2(e)). The particle separation behavior is determined by the design of the DLD devices. Using a pore size of 4 μm and varying pillar array gradients such that $\varepsilon = 1/N$, we developed a DLD system with critical diameters ranging from 700 nm to 2,000 nm, as determined based on Eq. 1.

This device has a very thin, single-stream input spanning 4 μm , which is sandwiched between two buffer streams (Fig. 2(c)). As particles flow through the device, they will be displaced until the DLD critical diameter is larger than the particle size. The sample particles will exit the device in various lateral positions based on their hydrodynamic sizes. As such, particles of less than 700 nm in size will not be laterally displaced from the sample stream, whereas particles larger

than 2,000 nm will remain in the stream until they reach the exit location corresponding to $D_c = 2,000$ nm. We initially calibrated the device with beads using the same method as in our previous works and found that the behavior of the DLD device was consistent with the established empirical model (see Supplementary Fig. S1). Additionally, to prevent contamination through the residual adsorption of NaCl ions into the PDMS, we completed all flow tests with various bead sizes at lower ionic concentrations before increasing the ionic concentration of the buffer. The ionic concentration was increased from 10 μM to 500 μM , and the values were selected based on the characteristic Debye length of the solution (see Supplementary Fig. S2). To change the buffer, DI water was used to flush the reservoir three times before new buffer was added.

The fabrication of the device uses standard photolithography techniques with deep reactive ion etching to fabricate the DLD channels. The fabrication diagrams and steps can be found in Supplementary Notes 3. The system is driven by a negative pressure at the outlet, whereas the sample and buffer inlets are open-air reservoirs to facilitate rapid changes of the ionic buffer inputs (see Supplementary Fig. S4).

A second DLD device was fabricated to test the limits and dynamic range of nanoparticle separation. The specifications for the second DLD device were all identical except for a reduction in the gap size to 2 μm . This reduction in gap size resulted in a separation range of 350 nm to 1,000 nm. These specifications can be derived from Eq. 1.

Samples and buffer solutions

The particles used in this study included NIST standard polystyrene beads (Bangs Laboratories, USA) ranging from 500 nm to 1,000 nm in size and fluorescence-coded polystyrene beads of 51 nm, 191 nm, 520 nm and 780 nm in size with excitation/emission wavelengths of 480/520 nm (Bangs Laboratories, USA). The beads were diluted in ultrapure 18 ohms filtered DI water (Millipore) by a factor of 10 and mixed in an ultrasonic bath for 5 min to reach a final concentration of 0.1% w/v.

The primary ionic salt used was sodium chloride, NaCl (Sigma, Singapore), dissolved in ultrapure DI water in concentrations ranging from 10 μ M to 500 μ M. The high salt buffer solution used was 1x phosphate buffered saline (PBS) solution (Sigma-Aldrich, Singapore), with a \sim 135 mM NaCl concentration. Non-ionic surfactant was prepared using Pluronic F-127 at 1 mM (Sigma, Singapore).

Experimental setup and data analysis

Pre-treatment of the devices was performed by applying a surface coating of (tridecafluoro-1,1,2,2-tetrahydrooctyl)-1-trichlorosilane (Sigma, Singapore) via chemical vapor deposition and a pre-flow treatment of 1% (w/v) Pluronic F-127 solution to prevent the attachment of bio-particles to the device surface. After 30 min of Pluronic treatment, the device was washed by loading fresh ultrapure DI water into the reservoirs and flushing for 30 min. To drive the flow process, a 100 μ l gas-tight Hamilton glass syringe was attached to a 150 μ m diameter tube, which, in turn, was inserted into the device outlet. A syringe pump (Chemyx) was attached to the syringe, and the syringe piston was retracted at a flow rate of 0.05 μ l/min. At this flow rate,

the beads were traveling at a velocity of approximately 250 $\mu\text{m/s}$ in the microfluidic device with a channel depth of 4 μm .

To capture the separated beads at the output of the DLD device, a high-speed Phantom camera (M310) was attached to a bright-field upright microscope at a magnification of 400x. Images of the NIST beads at the output positions were captured from each video, and the beads were counted manually from these images. A sample video is provided in the Supplementary Information. The lowest possible bead size that could be visually distinguished at 400x magnification and a 1280x800 pixel resolution was 500 nm. To capture fluorescence images, a CCD camera was used to capture the 520 nm wavelength emission of the green fluorescent nano-sized beads. The images were processed using ImageJ to convert the fluorescence intensities into grayscale images to measure the intensities and locations of the fluorescence streaks.

Results and Discussion

Apparent particle size in the dynamic DLD system

The electrostatic interactions between the particles and the device will impact the hydrodynamic particle size and drastically influence the separation of sub-micron particles and nanoparticles. Although the Debye length is commonly used to estimate the electrostatic influence on surfaces, we hypothesize that electrostatic forces beyond the Debye length are sufficient to induce nanoparticle displacements that can be detected by size-sensitive DLD systems. A model was established to predict the long-range repulsive electrostatic effects acting on DLD structures and particles (Fig. 1). Attractive electrostatic forces are not considered because the attraction of particles to surfaces would imply the possibility of physical or electrostatic attachment, thus preventing separation.

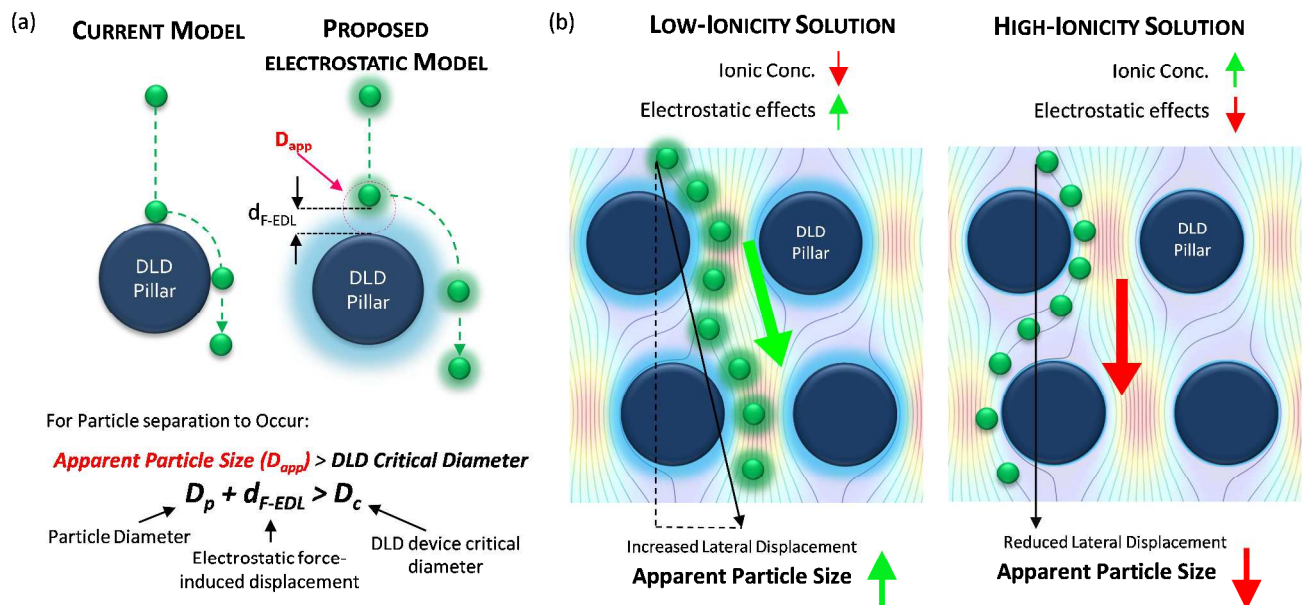


Fig. 1: An electrostatic force-modulated DLD system for variable apparent particle size separation: The schematics shown here depict the proposed model for electrostatic interactions between a DLD pillar wall and a particle (a). The value of D_{app} is determined by the sum of D_p and d_{F-EDL} . The separation of particles of the same size can result in two different outcomes; which outcome occurs is determined by the concentration of the fluid. Low (high) ionic concentrations in the fluid medium increase (decrease) the apparent particle size (D_{app}), as shown in (b). The fluid streamlines shown here were extracted from Comsol Multiphysics v4.1 modeling software.

Conventionally, DLD systems do not account for electrostatic effects (Fig. 1a). Particle separation is theoretically governed by the critical size at which separation occurs only if the particle size is greater than that critical size, namely, D_c (Eq. 1).

$$D_c = 1.4g\varepsilon^{0.48} \quad (\text{Equation 1})$$

where D_c is the critical particle diameter for separation; g is the gap or pore size between pillars; and ε is the slope of the pillar array ($\tan \theta = \varepsilon$), where θ is the angle of the pillar array gradient.

Our proposed approach introduces electrostatic interactions into the modeling of particle separation; in this case, the effective critical size for particle separation that applies in the DLD device due to electrostatic interactions is called the apparent particle size (D_{app}). D_{app} must be greater than the D_c of the DLD system for separation to occur such that:

$$D_p + d_{F-EDL} > D_c \quad (\text{Equation 2})$$

We can determine the apparent particle size (D_{app}) by summing particle diameter (D_p) and the displacement caused by electrostatic interactions between the particles and the surface of the DLD device (d_{F-EDL}). By modulating D_{app} , one can achieve different separation outcomes for

particles with the same D_p , as shown in Fig. 1b for an enhanced separation size and in Fig. 1c for a reduced separation size.

Because D_p is fixed, we can modulate D_{app} only by changing the electrostatic force-induced displacement d_{F-EDL} . Decreasing the ionic concentration of the buffer medium will increase the electrostatic force interactions between the particles and the device surface, which will, in turn, increase D_{app} . This increase in apparent particle size aids in the effective separation of smaller particles in pore-based microfluidic systems. The converse is true for an increase in the ionic concentration of the fluid medium (Fig. 1c), which causes a reduction in electrostatic effects that reduces D_{app} in the same microfluidic setup. Thus, the dynamic range of the device can be significantly modulated by tuning the electrostatic interaction variable d_{F-EDL} .

Separating nanoparticles under different ionic concentrations

To determine and understand the extent of electrostatic effects on modulating size-sensitive particle separation behavior from the microscale to the nanoscale, we first investigated the sub-micro regime before proceeding to the nano regime. We designed a DLD system with a large pore size of 4 μm and a pillar diameter of 6 μm (Fig. 2a). The device was fabricated using standard photolithography and etched to a depth of 4 μm (Fig. 2b). The particle sample and buffers are stored in open reservoirs and driven into the device by negative pressure. This design permits rapid changes of the buffer solutions in the reservoirs while ensuring a thin width of the sample stream sandwiched between two buffer streams (Fig. 2c). The DLD device is a multi-segmented device with 14 critical diameter segments, with each segment in a

continuous sequence (Fig. 2d). The gradient in each DLD segment increases such that each successive segment is responsible for the lateral displacement of particles with increasing D_c from 700 nm to 2,000 nm (Fig. 2e). The details of the experimental protocols can be found in the Methods section.

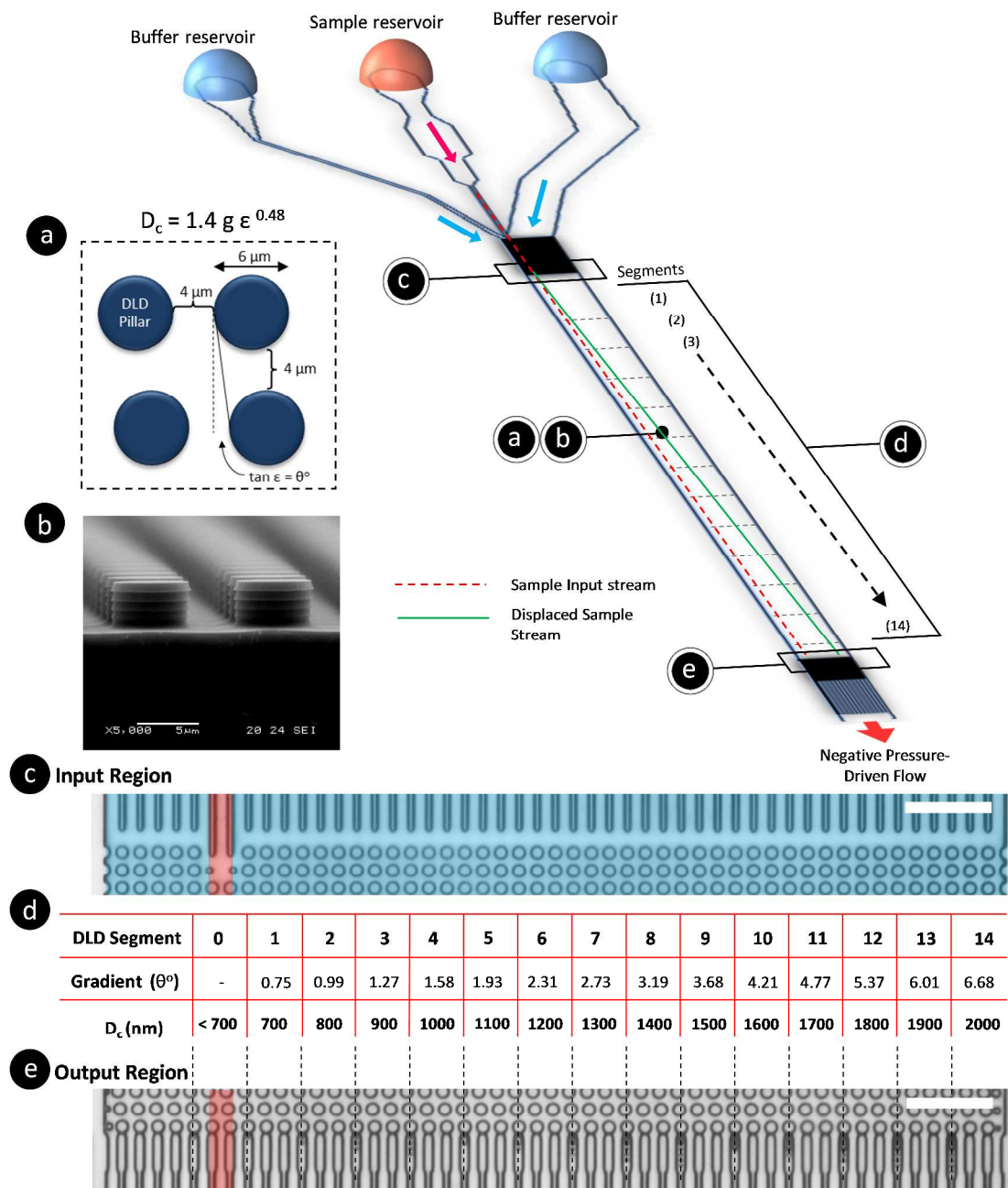


Fig. 2: Schematics of DLD device to test effects of electrostatic forces on particle separation. The DLD device was designed based on the formula in (a) and the scanning electron microscope image of the

deep reactive-ion-etched channels (b). The input region in (c) includes a thin sample stream in red and two buffer sheath flows in blue. The device is segmented into 14 serially connected sections (d), each of which has a fixed pillar gradient that corresponds to a specific D_c . The exit region of the device is divided into 15 sections (including the sample inlet stream) and 45 sub channels (e). All of the pillars in the device are 6 μm in diameter and have a 4 μm pore size. The scale bar represents 50 μm .

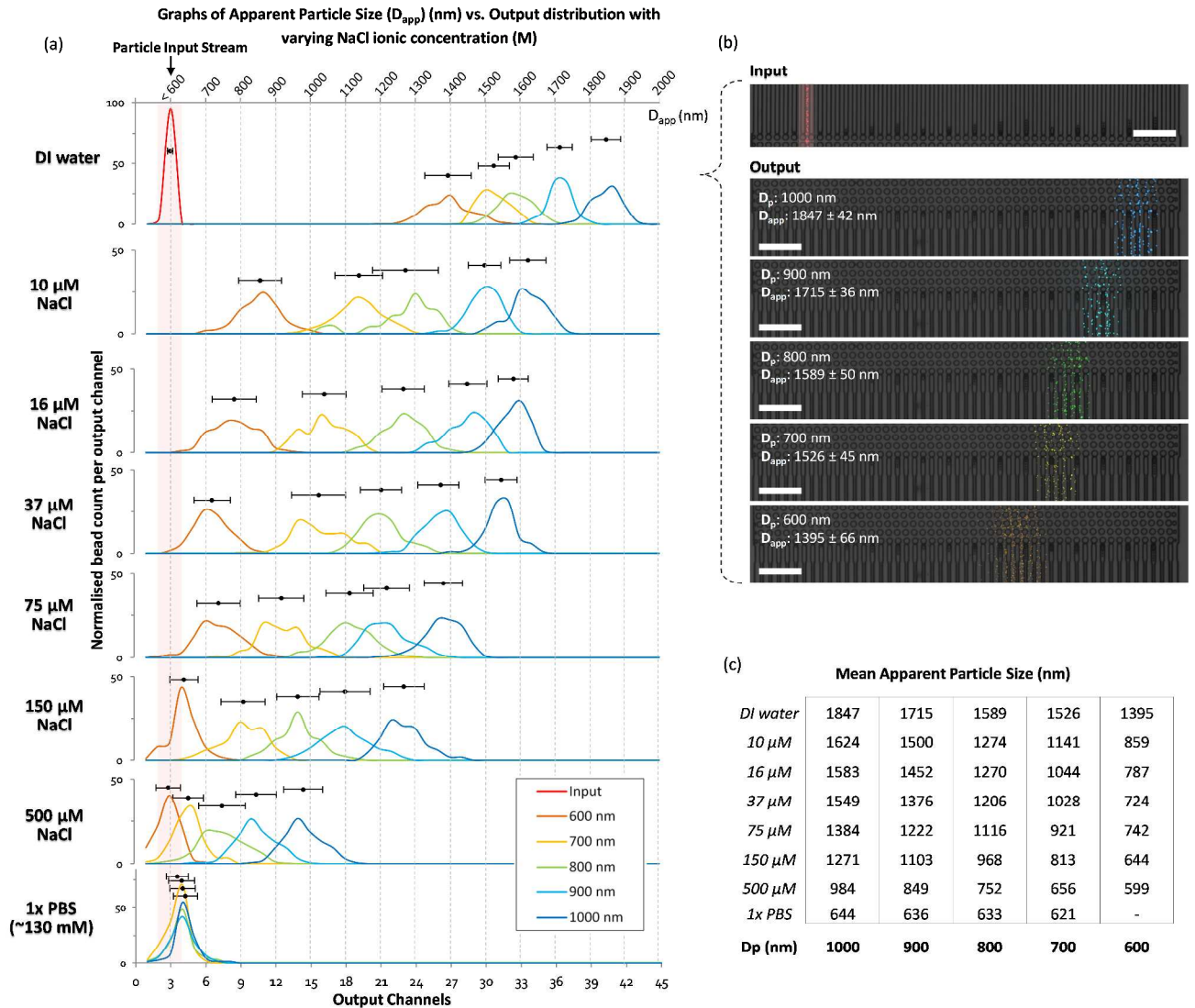


Fig. 3: DLD separation spectra of sub-micron particles in media with different ionic concentrations. The particle input stream is shown in (a) as a red line in the DI water spectrum and highlighted in the red region for the rest of the spectra. The separation spectra are marked in various colors: dark blue for 1,000 nm, sky blue for 900 nm, green for 800 nm, yellow for 700 nm, and orange for 600 nm. The output distributions are normalized individually. The top axis denotes D_{app} , which ranges from 700 nm to 2000 nm, and the bottom axis shows the output channels. Part (b) shows the particle separation in the raw video footage with pseudo-colors added to highlight the particles. The extracted information is overlaid on the image of the corresponding output channel. The raw footage can be seen in Supplementary Movie S1. The scale bars represent 50 μm. In (c), the mean displacement of the particles in different ionic NaCl concentrations is tabulated.

Beads of sizes ranging from 600 nm to 1,000 nm were tested in the DLD device in varying NaCl ionic buffer concentrations that varied from 10 μM to 500 μM. Ultrapure DI water was

used to test the effects of a non-ionic solution, and a 1x PBS solution at a pH of 7.4 was used to investigate the effects of a high salt solution. The separation results were plotted to show the variation in the apparent particle size with different ionic solutions (Fig. 3). Theoretically, when electrostatic considerations are ignored, the particles should exhibit a D_{app} close to D_p and should exit the DLD device from a segment corresponding to a size close to the D_c of the device (Supplementary Fig. S2). However, the apparent particle sizes in the DLD device significantly responded to changes in the ionic concentration of the buffer streams. Ultrapure DI water resulted in the most significant shift in the separation spectrum of the particles, with $D_p = 1,000$ nm particles exhibiting a D_{app} of 1,847 nm. Meanwhile, none of the particles that exhibited a D_{app} of less than 700 nm were separated from the input stream in the PBS buffer. Increasing the ionic concentration reduced the D_{app} of the particles, as hypothesized in Fig. 1. This phenomenon is unique and remarkable, because a simple manipulation of the ionic buffer can drastically shift the D_{app} of a 1,000 nm particle from a value of 1,847 nm to less than 700 nm. The lower boundary on D_{app} is unknown, as it is beyond the limits of the DLD particle separation range. The total variation in D_{app} that can be achieved by changing from a non-ionic to a highly ionic solution is greater than 114% for a 1,000 nm particle. This suggests that fine modulation of particle size separation behavior can be achieved by using optimized ionic concentrations. To our knowledge, this large variation in the apparent particle size during pore-based particle separation has never previously been observed, and thus, the results reported here represent the first quantitative measurements of this phenomenon using a DLD system.

At a 500 μ M concentration of NaCl, the ionic shielding sufficiently reduced the interaction such that D_{app} was comparable to the particle size predicted for DLD using Eq. 1. Using the

knowledge obtained by characterizing the modulation of the separation spectrum by electrostatic forces, we tested the limits of the device and found that it was able to effectively separate a sample mixture of nanoparticles of 190 nm, 520 nm and 780 nm in size (see Supplementary Fig. S3). In theory, conventional DLD systems can separate nanoparticles. However, previous attempts to separate nanoparticles of less than 500 nm in size in DLD systems have not been successful for pore sizes larger than $1 \mu\text{m}^{24}$. Here, we demonstrated distinct separation using a $4 \mu\text{m}$ DLD gap size and direct separation from a particle mixture.

Electrostatic force model vs. Debye length model

The DLD separation method is known for its high resolution and precision for particle separation. The inclusion of electrostatic forces in DLD, as suggested in the proposed model (Fig. 1), enables dynamic modulation of the size sensitivity for the separation of micro- and nanoparticles. The mean D_{app} is plotted against D_p in Fig. 4(a), wherein the dotted line represents the theoretical model in which electrostatic forces are neglected ($d_{\text{F-EDL}} = 0$). Data points above the dotted line suggest the presence of a positive repulsive electrostatic force due to $d_{\text{F-EDL}} > 0$, resulting in $D_{\text{app}} > D_p$. When $d_{\text{F-EDL}} < 0$, the force between the particles and the device surface becomes attractive and the apparent particle size becomes smaller than the actual particle diameter. This is probably caused by the onset of attractive van der Waals forces dominating the repulsive electrostatic forces at low Debye length scales of $\sim 1 \text{ nm}^{33}$. Particles suspended in ionic salt buffer media with NaCl concentrations lower than $500 \mu\text{M}$ appear to exhibit an increase in apparent particle size, whereas particles in ionic solutions with NaCl concentrations greater than $500 \mu\text{M}$ will exhibit a reduced apparent particle size in the DLD

device. Because the lower limit on D_c for the empirical model of the DLD system is 700 nm, we are unable to accurately predict a reduction in the apparent particle size to less than 700 nm. Certainly, a salt concentration of greater than 200 mM will induce an average reduction in apparent particle size in the DLD system of more than 263 nm.

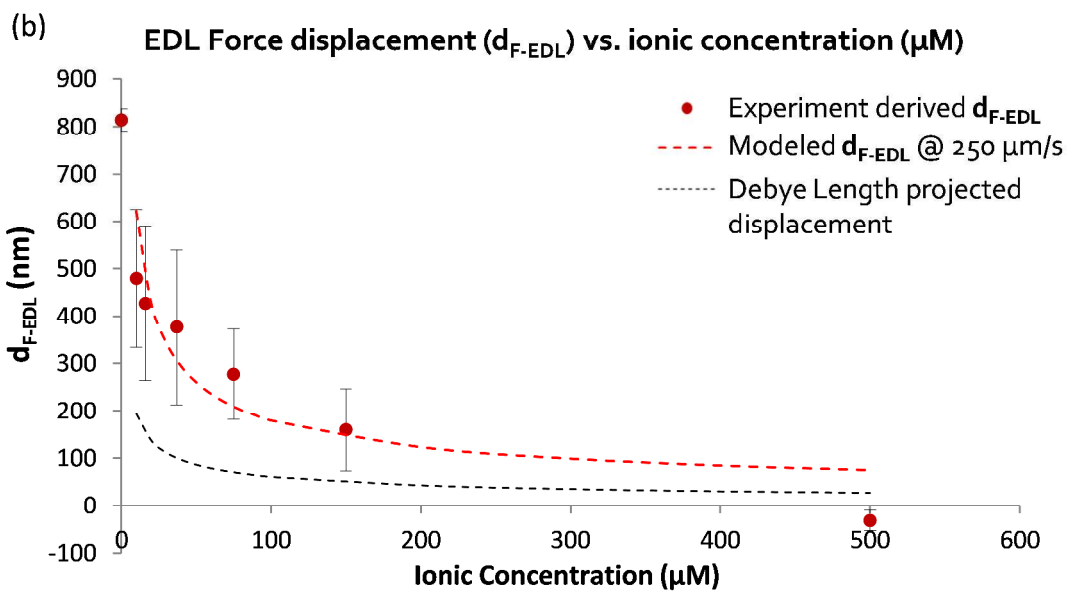
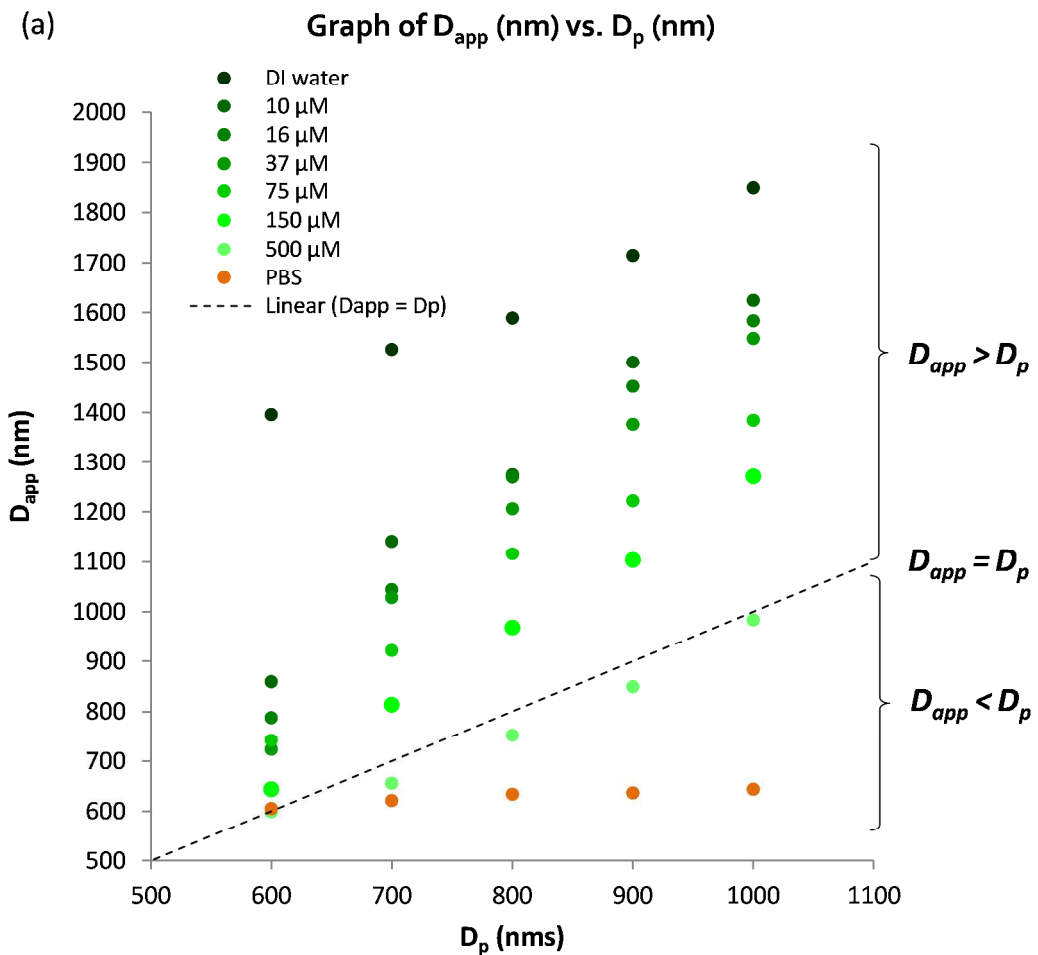


Fig. 4: Measurement and derivation of the apparent particle size (D_{app}): Part (a) shows how the tabulated average D_{app} varies with respect to the particle diameter. The dotted line shows where the D_{app} is the same as the actual particle diameter (D_p). D_{app} is the sum of D_p and d_{F-EDL} . The electrostatic force-induced displacement (d_{F-EDL}) for ionic concentrations between 0 and 500 μM is represented by red points (c). The red-dotted lines show the predicted enhanced displacement (d_{F-EDL}) from the Equation (1).

In this pioneering study of the quantitative effects of electrostatic forces on DLD nanoparticle separation, we limit the electrostatic effects included in the model to the repulsive electrostatic forces acting in solutions with ionic concentrations below 500 μM NaCl. Attractive electrostatic forces would cause the nanoparticles to attach to the walls, forming aggregated particles, and would reduce the apparent particle size to a sufficient extent that particle separation would become impossible. A more detailed derivation of d_{F-EDL} and a further explanation can be found in Supplementary Information S4 and S5. The electrostatic interaction between the nanoparticles and the DLD pillars is described as follows:

$$d_{F-EDL} = -\lambda_D \ln \left[\frac{-\sigma_p^2 \sigma_s^2 + \sqrt{\sigma_p^4 \sigma_s^4 + \frac{(\sigma_p^2 + \sigma_s^2)^3 \mu \epsilon_0 \epsilon_r V_{bulk}}{\lambda_D}}}{\sigma_p^2 + \sigma_s^2} \right] \quad (\text{Equation 2})$$

Here, the electrostatic force displacement d_{F-EDL} is dependent on the Debye length (λ_D), the electrical permittivities of the medium (ϵ) and free space (ϵ_0), the surface charge densities of the particles (σ_p) and the device surface (σ_s), the viscosity of the fluid (μ) and the velocity of the surrounding fluid (V_{bulk}). Surprisingly, d_{F-EDL} is predicted to be independent of particle size and dependent only on the charge density, ionic strength and fluid velocity (Eq. 2). Because the physical size of each particle is fixed and the electrostatic component of the force, d_{F-EDL} , is variable, we plot the average d_{F-EDL} against the ionic concentration from 0 to 500 μM (Fig. 4b). The average experimental d_{F-EDL} values were calculated by subtracting the particle diameter

from the apparent particle size at various concentrations. The modeled d_{F-EDL} results (red dotted line) at a fluid flow velocity of 250 $\mu\text{m/s}$ are largely in agreement with the experimental values. The conventional Debye length approximation for nanoparticle separation (black dotted line) deviates from the proposed model by more than 100% (Fig. 4b). Thus, our model predicts that long-range electrostatic forces acting on nanoparticles cannot be assumed to be negligible in ionic media with concentrations lower than 500 μM . A slight change in the ionic medium will have a significant effect on the apparent size of the nanoparticles.

Expanded dynamic range for nano- to microparticle separation

To build on the results presented above by investigating the electrostatic influence and the limits on nanoparticle size manipulation in large-pore DLD devices, we designed and fabricated a new DLD device with a smaller gap size of 2.0 μm (see Fig. 5a and Supplementary Fig. S6). This device offers a separation spectrum with D_c values ranging from 350 nm to 1000 nm in steps of 50 nm. The electrostatic force-dependent DLD separation was tested using fluorescent polystyrene beads of 51 nm and 190 nm in size. Using a sheath flow of ultrapure DI water, we succeeded in distinctly separating these particles from the original flow stream (Fig. 5b). To our knowledge, the ability to separate 51 nm particles using a 2.0 μm pore-based filter is unprecedented. The pore-to-particle size ratio is approximately 40, greater than that of Regtmeier et al., who achieved a pore-to-particle size ratio of 33.

The 51 nm and 190 nm particles exhibited D_{app} values of 650 nm and 910 nm, respectively. The mean D_{app} difference was 260 nm, compared with a D_p size difference of 139 nm – an 87% greater size difference between the particles. The separation spectrum presented in Fig. 5a

shows a shift toward the left side of the scale bar, indicating a dynamic increase in D_{app} that enabled particles of smaller D_p to be separated in the same DLD device. In a conventional DLD model (Eq. 1), separating 51 nm particles would require an impractical 2-meter-long device with a channel width of 0.5 mm.

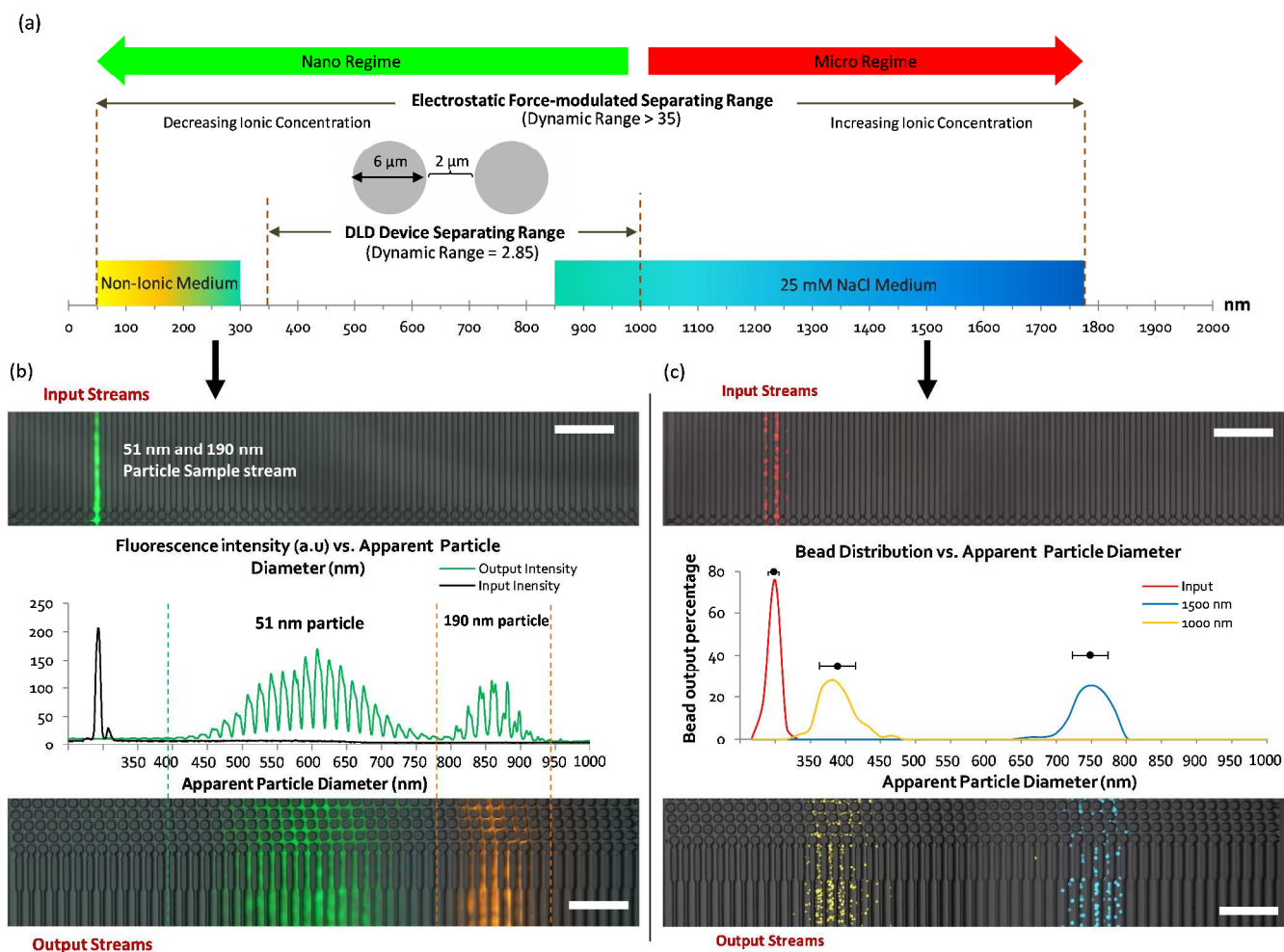


Fig. 5: Nanoparticle separation limits and dynamic ranges for a device with 2 μm pores. A new DLD device with a pore size of 2 μm and pillar size of 6 μm used for nanoparticle separation with an increased dynamic range is shown in (a). Sample particles were tested in the DLD system, and 51 nm (green) and 190 nm (orange) particles were found to exhibit a distinct separation, with very little overlap in the spectrum (b). Pseudo-color was added to make the particle streams appear distinct. A microparticle separation regime in the same device was created using a NaCl solution with a higher ionic concentration (25 mM) for 1000 nm (yellow) and 1500 nm (blue) particles (c). All particle color streams are pseudo-colors.

The separation spread and distribution of the 51 nm particles were relatively wide, with a standard deviation of approximately 125 nm, greater than the size of the particles themselves. This was due to the diffusion of the particles. At a flow rate of 250 $\mu\text{m/s}$, the diffusion length $l = \sqrt{2Dt}$ of the flow stream is approximately 100 μm . Therefore, the DLD nanoparticle separation resolution is limited only by diffusion. Moreover, the fabrication of the device pillars using DRIE introduced scalloping effects (Fig. 2b), which may have introduced microscale variations in fluid flow, resulting in a reduced DLD separation efficiency.

To test the other extreme of the separation range in the same device, a high-ionicity medium consisting of a 25 mM NaCl solution was used for the separation of 1,000 nm and 1,500 nm particles. Fig. 5c shows the particle separation distribution with added pseudo-color. The separation of the particles is distinct, with D_{app} values of 441 nm and 801 nm for the 1,000 nm and 1,500 nm particles, respectively, and an average of $d_{\text{F-EDL}} = -630$ nm, indicating a decrease in the apparent particle size. Hence, using the same DLD device, a 1000 nm particle can appear “smaller” than a 51 nm particle in a different ionic medium.

The electrostatic modulation of nanoparticle sizes enables unprecedented continuous nanoparticle separation and increases the effective dynamic range of pore-based DLD systems for separation from 2.85 to 35. Moreover, it also allows for the separation of particles with different sizes using the same device while outperforming conventional bench-top centrifuge methods (Supplementary Fig. S7). We compared the separation of 51 nm particles in a conventional bench-top centrifuge at 22,000g and were unable to fully separate these particles from the original fluid sample.

Response time for real-time nanoparticle separation manipulation

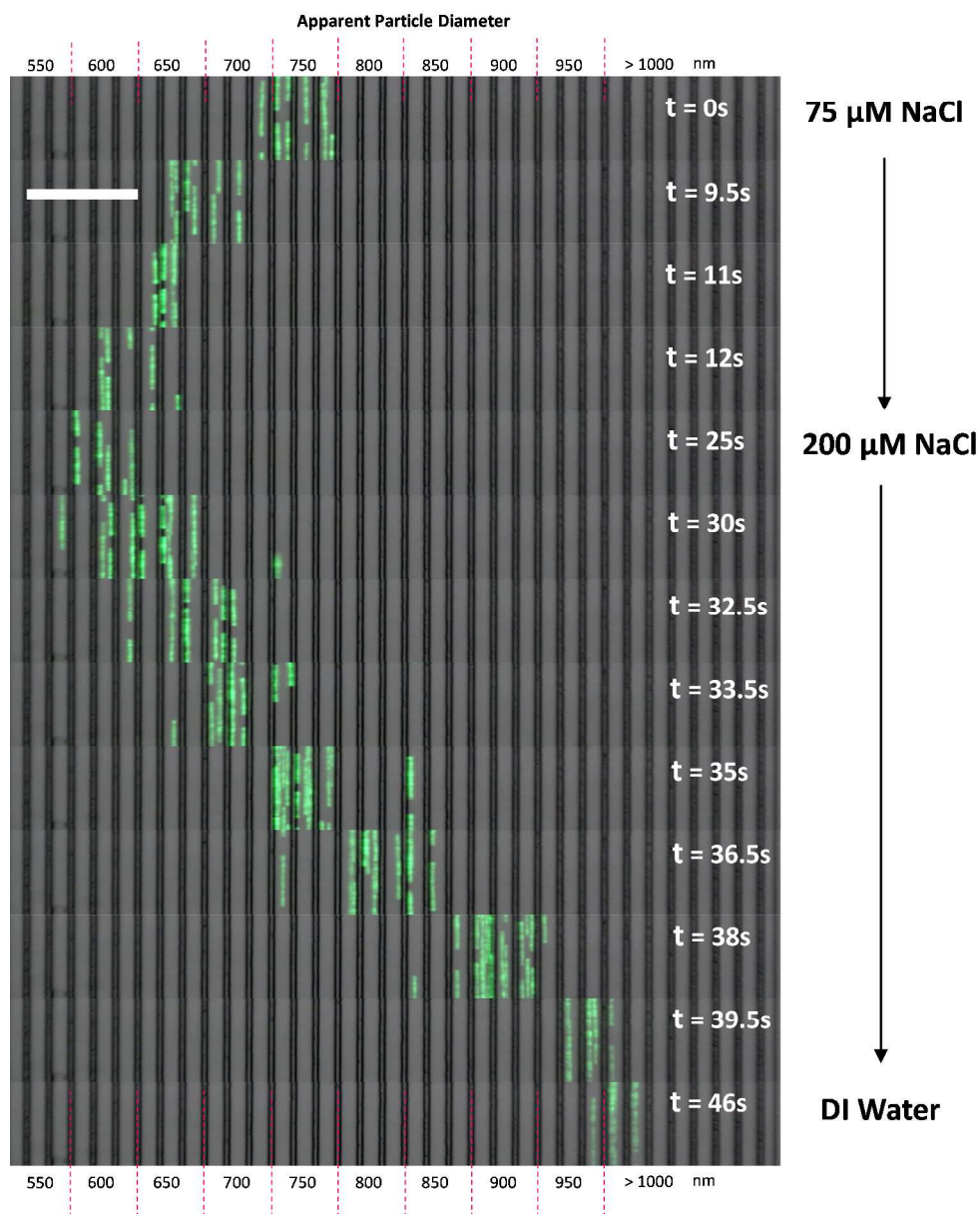


Fig. 6: Response time test for real-time particle separation manipulation. 500nm beads were used as test beads for response time in the separation test. Screen capture from video footages were extracted and sequenced from 0s to 46s (see Supplementary Movie 1). Salt solutions in buffer reservoirs were changed in real-time and the separation of beads were observed under a microscope using a video camera. The white bar depicts a 40 μm distance.

To our knowledge, a passive flow (non-external force-field-based) method for the real-time manipulation of nanoparticle separation has never before been achieved. Most real-time separation involves centrifugal, electric, acoustic or magnetic fields. These systems require

additional equipment or experimental setups to enable fine control of the particle separation behavior. Although Arosio et al. used a microfluidic centrifuge system for the separation of 50 nm to 200 nm particles, the setup was not a continuous flow system and the separation spectra considerably overlapped¹⁸. Using a combination of EDL effects, electrokinetics and nano-fabrication, Regtmeier et al. successfully separately nanoparticles of 15 nm and 36 nm in size³¹. Here, we demonstrated that by simply changing the buffer solutions in the reservoirs of our system, it is possible to control the separation of nanoparticles with a response time of 20 seconds or less (Fig. 6 and Supplementary Movie 2).

To test the real-time separation response of ionic buffer separation, 500 nm fluorescent beads were tested in three different buffer solutions, as shown in Fig. 6. To capture video fluorescence images, a 5D Mark III DSLR camera was used at ISO 25600 at 1/30 fps. A bright-field image of the channels was overlaid on the fluorescence video. Thus, the effects of real-time changes to the ionic buffers were captured (see Supplementary Movie 2).

A 75 μM NaCl solution was used as the initial buffer, and the fluorescent particle stream settled within an apparent diameter range of 700 nm to 800 nm. Then, a 200 μM NaCl solution was flushed into the buffer reservoirs at $t = 0$ s. When the 200 μM NaCl solution was introduced, it took approximately 12 seconds for the full effect of the ionic solution to shift the separation spectrum of the particles to an apparent diameter range of 600 nm to 650 nm. However, when DI water was flushed into the reservoirs, the particle stream shifted in the opposite direction to apparent diameters of more than 1000 nm. This shift required approximately 20 seconds as the DI water flushed the NaCl solution out of the device.

This response time is dependent on the flow velocity of the fluids in the channel, which governs the time required to flush the previous buffer out of the system. Reducing the response time

would be possible with much higher flow velocities, which would also increase the throughput of separation. However, as seen from Eq. 2 and Supplementary Fig. S5, the apparent particle size would simultaneously decrease due to higher hydrodynamic drag forces opposing the electrostatic force. Despite this reduction in D_{app} , our model still exhibits a greater electrostatic influence compared with the Debye length approximation at microfluidic velocities as high as 10,000 $\mu\text{m/s}$.

Because ions can diffuse into surrounding channels consisting of PDMS and silicon, we did observe that prolonged use of high-ionicity solutions in PDMS-covered channels resulted in a less effective response because the ions were able to diffuse and accumulate in the PDMS channels. Hence, even if ultrapure DI water is used, the effects may be reduced as a result of residual NaCl ions in the PDMS diffusing back into the fluid medium.

Conclusion

By virtue of its sensitivity to particle size, DLD microfluidics is a promising separation method with potential applications including blood purification^{34,35}, bacteria separation^{36,37}, cancer cell concentration³⁸, etc²³. The high-throughput scalability of its fluid flow rates toward ml/min enables its application in a regime similar to that of traditional centrifugal methods. Although DLD using large-pore structures ($\sim 1.4 \mu\text{m}$) has demonstrated promise for the distinct, passive separation of sub-micron particles (600 nm – 1000 nm)²¹, separating particles of less than 500 nm in diameter has proven to be challenging because of additional relevant variables such as diffusion and electrostatic forces^{24,39}. To address these effects, in this study, we investigated a long-range EDL electrostatic model for DLD. By considering the electrostatic forces arising due

to the ionic strength of the buffer medium, our model uniquely accounts for the electrostatic forces between the surfaces of the DLD pillars and the particles, resulting in modifications to the apparent particle size and allowing for the simple and precise prediction of the induced displacement. Based on this model, the particle-wall interaction forces can be manipulated by tuning the ionic strength of the surrounding fluid, thereby enabling real-time manipulation of the particle size and separation without using magnetic, acoustic or electric fields. Accordingly, the separation of 51 nm particles using a micro-fabricated device with large pores of 2 μm in size was achieved. Moreover, we demonstrated continuous flow nano-separation with dynamic control of the separation spectrum, ranging from 51 nm to 1,500 nm, in a DLD device. The dynamic range for particle separation was thus increased by $\sim 1200\%$ in comparison with that of conventional DLD separation. The results of our approach represent the first demonstration of real-time, label-free nano-separation in a continuous flow microfluidic system, and the simplicity of this method provides an opportunity for rapid, distinct, high-throughput separation of synthetic nanoparticles or biologically relevant samples such as viruses, exosomes, proteins and DNA³⁹.

Acknowledgement

We would like to acknowledge the funding support from National University of Singapore (NUS), Singapore Institute for Neurotechnology (SINAPSE), and Ministry of Education Academic Research Fund (AcRF: R-397-000-183-112, R-397-000-153-112). The experiments were mostly performed in Cellular and Molecular Bioengineering labs in NUS. We also would like to thank Dr Shashi Ranjan for the useful discussions for the study of study solute ionic effect in DLD separation. Post graduate PhD student Wang Ming Kevin assisted in the confirmation of the formulation and model of electrostatic DLD.

Author contribution

K.K.Z, Y.Z., C.H.C conceived the idea and designed the experiments. K.K.Z performed the experiments and wrote the paper. K.K.Z, N.V.T., Y.Z, C.H.C. analyzed the results and revised the paper.

Competing financial interests

There are no competing financial interests for the duration of the experiment.

References

- 1 Nie, Z., Petukhova, A. & Kumacheva, E. Properties and emerging applications of self-assembled structures made from inorganic nanoparticles. *Nat Nano* **5**, 15-25.
- 2 Rahman, I. A., Vejayakumaran, P., Sipaut, C. S., Ismail, J. & Chee, C. K. Size-dependent physicochemical and optical properties of silica nanoparticles. *Materials Chemistry and Physics* **114**, 328-332.
- 3 Yu, Q., Qi, L., Mishra, R. K., Zeng, X. & Minor, A. M. Size-dependent mechanical properties of Mg nanoparticles used for hydrogen storage. *Applied Physics Letters* **106**, 261903.
- 4 Zhang, S., Li, J., Lykotrafitis, G., Bao, G. & Suresh, S. Size-Dependent Endocytosis of Nanoparticles. *Advanced materials (Deerfield Beach, Fla.)* **21**, 419-424.
- 5 De, M., Ghosh, P. S. & Rotello, V. M. Applications of Nanoparticles in Biology. *Advanced Materials* **20**, 4225-4241.
- 6 Salata, O. Applications of nanoparticles in biology and medicine. *Journal of nanobiotechnology* **2**, 3.
- 7 Wang, E. C. & Wang, A. Z. Nanoparticles and their applications in cell and molecular biology. *Integrative Biology* **6**, 9-26.
- 8 Stark, W. J., Stoessel, P. R., Wohlleben, W. & Hafner, A. Industrial applications of nanoparticles. *Chemical Society reviews*.
- 9 Kowalczyk, B., Lagzi, I. & Grzybowski, B. A. Nanoseparations: Strategies for size and/or shape-selective purification of nanoparticles. *Current Opinion in Colloid & Interface Science* **16**, 135-148.
- 10 Laue, T. M. & Stafford III, W. F. MODERN APPLICATIONS OF ANALYTICAL ULTRACENTRIFUGATION. *Annual Review of Biophysics and Biomolecular Structure* **28**, 75-100.
- 11 Fagan, J. A., Becker, M. L., Chun, J. & Hobbie, E. K. Length Fractionation of Carbon Nanotubes Using Centrifugation. *Advanced Materials* **20**, 1609-1613.
- 12 Vauthier, C., Cabane, B. & Labarre, D. How to concentrate nanoparticles and avoid aggregation? *European journal of pharmaceutics and biopharmaceutics : official journal of Arbeitsgemeinschaft fur Pharmazeutische Verfahrenstechnik e.V* **69**, 466-475.
- 13 Lenshof, A. & Laurell, T. Continuous separation of cells and particles in microfluidic systems. *Chemical Society reviews* **39**, 1203-1217.
- 14 Pamme, N. Continuous flow separations in microfluidic devices. *Lab on a chip* **7**, 1644-1659.
- 15 Hammarstrom, B., Laurell, T. & Nilsson, J. Seed particle-enabled acoustic trapping of bacteria and nanoparticles in continuous flow systems. *Lab on a chip*.
- 16 Collins, D. J., Alan, T. & Neild, A. Particle separation using virtual deterministic lateral displacement (vDLD). *Lab on a chip* **14**, 1595-1603.
- 17 Hanauer, M., Pierrat, S., Zins, I., Lotz, A. & Sonnichsen, C. Separation of nanoparticles by gel electrophoresis according to size and shape. *Nano Lett* **7**, 2881-2885.
- 18 Arosio, P., Müller, T., Mahadevan, L. & Knowles, T. P. J. Density-Gradient-Free Microfluidic Centrifugation for Analytical and Preparative Separation of Nanoparticles. *Nano Letters* **14**, 2365-2371.
- 19 Prabhu, A. S. *et al.* Chemically modified solid state nanopores for high throughput nanoparticle separation. *Journal of physics. Condensed matter : an Institute of Physics journal* **22**, 454107.
- 20 Stavis, S. M., Geist, J. & Gaitan, M. Separation and metrology of nanoparticles by nanofluidic size exclusion. *Lab on a chip* **10**, 2618-2621.
- 21 Huang, L. R., Cox, E. C., Austin, R. H. & Sturm, J. C. Continuous particle separation through deterministic lateral displacement. *Science* **304**, 987-990.
- 22 Beech, J. P., Jonsson, P. & Tegenfeldt, J. O. Tipping the balance of deterministic lateral displacement devices using dielectrophoresis. *Lab on a chip* **9**, 2698-2706.

- 23 McGrath, J., Jimenez, M. & Bridle, H. Deterministic lateral displacement for particle separation: a review. *Lab on a chip* **14**, 4139-4158.
- 24 Santana, S. M., Antonyak, M. A., Cerione, R. A. & Kirby, B. J. Microfluidic isolation of cancer-cell-derived microvesicles from heterogeneous extracellular shed vesicle populations. *Biomedical microdevices* **16**, 869-877.
- 25 Chen, Y. *et al.* Concentrating Genomic Length DNA in a Microfabricated Array. *Physical review letters* **114**, 198303.
- 26 López-García, J. J., Horno, J. & Grosse, C. Poisson–Boltzmann Description of the Electrical Double Layer Including Ion Size Effects. *Langmuir : the ACS journal of surfaces and colloids* **27**, 13970-13974.
- 27 Haywood, D. G., Saha-Shah, A., Baker, L. A. & Jacobson, S. C. Fundamental Studies of Nanofluidics: Nanopores, Nanochannels, and Nanopipets. *Analytical chemistry* **87**, 172-187.
- 28 Zeng, Y. *et al.* Effect of particle size and Debye length on order parameters of colloidal silica suspensions under confinement. *Soft Matter* **7**, 10899-10909.
- 29 Krishnan, M., Mojarad, N., Kukura, P. & Sandoghdar, V. Geometry-induced electrostatic trapping of nanometric objects in a fluid. *Nature* **467**, 692-695.
- 30 Fu, J., Schoch, R. B., Stevens, A. L., Tannenbaum, S. R. & Han, J. A patterned anisotropic nanofluidic sieving structure for continuous-flow separation of DNA and proteins. *Nature nanotechnology* **2**, 121-128.
- 31 Regtmeier, J., Kasewieter, J., Everwand, M. & Anselmetti, D. Continuous-flow separation of nanoparticles by electrostatic sieving at a micro-nanofluidic interface. *Journal of separation science* **34**, 1180-1183.
- 32 Davis, J. A. *Microfluidic Separation of Blood Components through Deterministic Lateral Displacement* Doctor of Philosophy thesis, Princeton University, (2008).
- 33 Butt, H.-J. Measuring electrostatic, van der Waals, and hydration forces in electrolyte solutions with an atomic force microscope. *Biophysical journal* **60**, 1438-1444.
- 34 Davis, J. A. *et al.* Deterministic hydrodynamics: taking blood apart. *Proceedings of the National Academy of Sciences of the United States of America* **103**, 14779-14784.
- 35 Zeming, K. K., Ranjan, S. & Zhang, Y. Rotational separation of non-spherical bioparticles using I-shaped pillar arrays in a microfluidic device. *Nat Commun* **4**, 1625.
- 36 Ranjan, S., Zeming, K. K., Jureen, R., Fisher, D. & Zhang, Y. DLD pillar shape design for efficient separation of spherical and non-spherical bioparticles. *Lab on a chip* **14**, 4250-4262.
- 37 Morton, K. J. *et al.* Crossing microfluidic streamlines to lyse, label and wash cells. *Lab on a chip* **8**, 1448-1453.
- 38 Louthback, K. *et al.* Deterministic separation of cancer cells from blood at 10 mL/min. *AIP Advances* **2**, -.
- 39 Sturm, J. C., Cox, E. C., Comella, B. & Austin, R. H. Ratchets in hydrodynamic flow: more than waterwheels. *Interface focus* **4**, 20140054.